Processing and Application of Ceramics 13 [2] (2019) 115–123

https://doi.org/10.2298/PAC1902115L

Reactions between Si melt and various ceramics

Che-Yu Lin[1], Kun-Lin Lin[2,*], Chien-Cheng Lin[1,*]

[1]*Department of Materials Science and Engineering, National Chiao-Tung University, Hsinchu, Taiwan*
[2]*National Nano Device Laboratories, National Applied Research Laboratories, Taiwan*

Received 1 August 2018; Received in revised form 7 December 2018; Accepted 13 March 2019

Abstract

Reactions between different kinds of ceramics and silicon were studied to evaluate ceramics as candidates for their use in the process of silicon-crystal growth. Three types of ceramic plates, Al_2O_3, ZrO_2 and quartz (SiO_2), were put into contact with a silicon wafer via annealing at 1450 °C for 30 min under an Ar atmosphere. Defects appeared at the Si-ceramics interface. Among these, a crack and a dislocation pile up were found at the Si-SiO_2 dissolution couple. In addition, two intermetallic compounds, $Y_2Si_2O_7$ and Zr-Si, produced by the diffusion of Y, O and Zr from the ZrO_2 into the Si, were found at the Si-ZrO_2 dissolution couple. At the interface of the Si-Al_2O_3 dissolution couple, no intermetallic compounds and few defects were found. The oxygen concentration and electrical resistivity near the interface were high and gradually decreased away from the interface for all Si-ceramics dissolution couples.

Keywords: *ceramic crucible, silicon, interface, Si dissolution couple, crystal growth*

I. Introduction

The floating zone technique and Czochralski pulling technique (CZ) are relatively popular single-crystal growth methods. [1] Modern integrated circuits and electronic devices are mainly manufactured using single-crystal silicon wafers produced by CZ. The CZ method is primarily based on crystal-pulling from Si melt, for which a quartz crucible is placed in the hot zone to melt the polysilicon. During the thermal-pulling process, because the quartz crucible will soften at high temperatures, the crucible requires to be secured by a graphite crucible to prevent deformation. It was previously found that many kinds of defects are generated in the silicon ingot after the thermal process, such as vacancies, interstitial defects, oxidation-induced stacking faults and pits because oxygen from the quartz crucible, comprising silicon and oxygen, diffuses into the silicon ingot [1–7].

Quartz is a mineral comprising of silicon and oxygen atoms in a continuous silicon–oxygen (SiO_4) tetrahedral framework, with each oxygen being shared between two tetrahedra, which represents an overall chemical formula of SiO_2. The microstructure of the Si-SiO_2 interface was previously characterized using scanning electron microscopy (SEM) and it was found that the solution-precipitation mechanism causes Si inclusions and worm-like cristobalite SiO_2 to appear locally at the interface [8]. Local cristobalite SiO_2 formation can easily result in a crack formation at the surface of Si. Huang *et al.* [9,10] found that when the Ba concentration in silica glass was >30 ppm, the cristobalite SiO_2 changes to a dense, smooth, and continuous layer, which results in the reduction of the precipitation of Si inclusions and defects. The formation mechanism of the Ba-doped cristobalite layer is considered to be a heterogeneous nucleation caused by Ba additives. In addition to Ba additives, high-purity silica or Si_3N_4 coatings on the crucible significantly affect the lifetime of the Si ingots. A high-purity silica coating layer on the crucible is likely to act as a diffusion barrier layer and improve the ingot quality [11].

Nowadays, most crucibles used for Si single-crystal growth are made from silicon oxide (quartz). In this study, three types of alternative ceramic materials for use in Si crystal growth were proposed. In addition to quartz, for comparison, Al_2O_3 and ZrO_2 plates were put into contact with Si wafers. The microstructure of the Si-ceramics interfaces was characterized using transmission electron microscopy (TEM) in conjunction with energy dispersive spectroscopy (EDS). The concentration of oxygen and resistivity of the Si after the contact with the ceramics were also measured.

* Corresponding author: tel: + 886 3 5726 100,
e-mail: *kllin@narlabs.org.tw* (K.-L. Lin)
e-mail: *chienlin@faculty.nctu.edu.tw* (C.-C. Lin)

II. Experimental procedure

In order to simulate the reaction between the Si melt and the ceramics, Si wafers (diameter thickness ≈655–695 μm, O content ≈12.00–15.00 ppm) and ceramic plates of commercial Al_2O_3, quartz and 3 mol% Y_2O_3-stabilized ZrO_2 (thickness ≈2 mm), were cut into squares of 20 × 20 mm^2. After grinding and polishing both sides of the ceramics, the samples were placed in a rectangular graphite crucible with an inner diameter of 20 × 20 × 20 mm^3 and an outside diameter of 25 × 25 × 25 mm^3. Several pieces of silicon were then inserted in the crucible, as shown in the schematic in Fig. 1a. For the oxygen content and resistivity measurements, after contact between the Si and the ceramics, the pieces of Si were cut along a direction longitudinal to the interface, as shown in Fig. 1b. Figure 1c shows a photograph of the 20×20 mm^2 pieces of Si, 20×20 mm^2 pieces of quartz and a graphite crucible. The crucibles containing the Si-ceramics samples were placed in a vacuum furnace, evacuated to ≈10^{-6} Torr, and annealed at 1450 °C (which is slightly higher than the melting temperature of silicon at 1414 °C). After holding this temperature for 30 min, the furnace was allowed to cool down to room temperature, and the graphite crucibles were then removed.

The microstructural characterization of the Si-ceramics interface was characterized using a TEM (JEM 2010Fx, JEOL Ltd., Tokyo, Japan) equipped with an EDS (Model ISIS300, Oxford Instrument Inc., London, U.K.) and a scanning electron microscope (JSM 6500-F, JEOL Ltd., Tokyo, Japan) with an EDS attachment (X-Max 80, Oxford Instrument Inc., London, U.K.). The crystal structure of the reaction products at the interface was characterized by selected area diffraction patterns (SADP) of TEM and EDS. The Inorganic crystal structure database (ICSD), Joint Committee on Powder diffraction standards database (JCPDS) and the crystallographic software (Diamond version 3.0 and CaRIne Crystallography 3.1) were used for the identification of the crystal structures of the phases. The cross-sectional TEM specimens of Si-ceramics joints were prepared by conventional mechanical polishing and focused ion beam (FIB, FEI NovaLab 600). The quantitative composition analyses were performed based on the principle of the Cliff-Lorimer [12] standard-less method. Besides, in order to accurately calculate the lattice parameters of reaction products, the image magnification of TEM was calibrated using the MAG*I*CAL reference standard sample, Norrox Scientific Ltd. The pieces of Si from Si-ceramics joints were cut along a direction longitudinal to the interface shown in Fig. 1b for the residual oxygen and resistivity measurements. The concentration evaluation of the residual oxygen in Si by Fourier-transform infrared spectroscopy (FTIR, Bruker VERTEX 70) has been performed based on ASTM F 1188 method [13] and the resistivity of Si was measured by four-point probe resistance meter (RT-80, Napson Corporation, Tokyo, Japan).

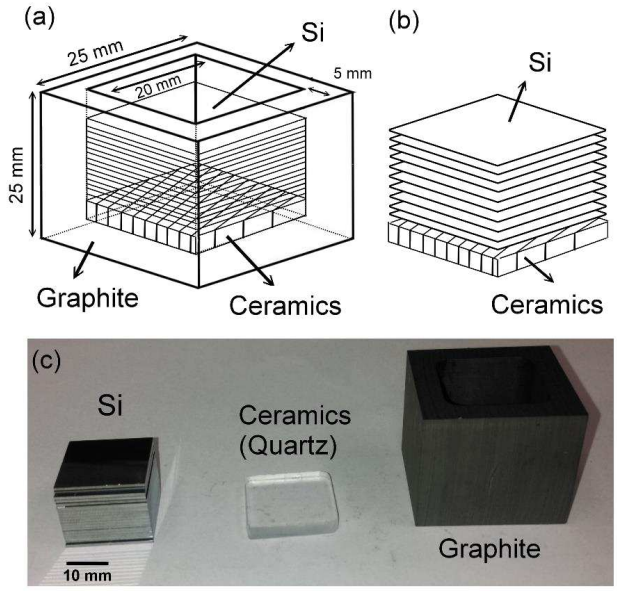

Figure 1. Schematic of the graphite crucible and the Si-ceramics contact (a), several pieces of Si cut along the direction longitudinal to the interface after contact (b), and photograph of pieces of Si, ceramics (quartz) and the graphite crucible (c)

III. Results and discussion

Figure 2 shows photographs of cross-sections of Si-SiO_2 (quartz), Si-ZrO_2 and Si-Al_2O_3 contacts after cutting. It can be seen that cracks appear in both the Si/SiO_2 (quartz) and Si/ZrO_2 samples due to a coefficient of thermal expansion (CTE) mismatch (CTE_{Si} ≈ 3–5 × 10^{-6} K^{-1}, CTE_{ZrO_2} ≈ 12 × 10^{-6} K^{-1}, CTE_{SiO_2} ≈ 8–14 × 10^{-6} K^{-1}, $CTE_{Al_2O_3}$ ≈ 8.1 × 10^{-6} K^{-1}); however, this phenomenon is not applicable for the Si-Al_2O_3 sample. Figure 3a and 3b show the SEM backscattered electron image (BEI) of the Si-SiO_2 dissolution couple after annealing at 1450 °C for 30 min, indicating that no reactional phase appeared at the interface and the interfacial profile not being smooth. An Si inclusion (shown in light contrast) and a worm-like SiO_2 (shown in dark contrast), were clearly seen at the silica-silicon interface, which is supported by the solution-precipitation

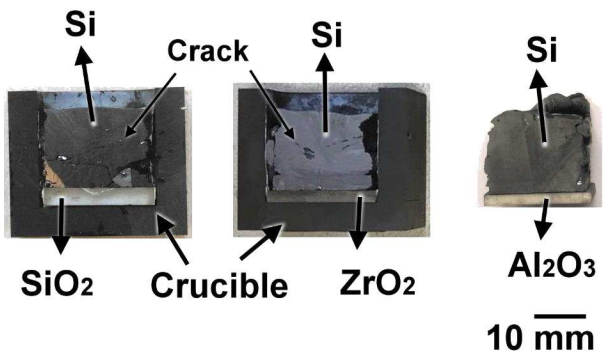

Figure 2. Photographs of the cross-sections of the Si-SiO_2 (quartz), Si-ZrO_2 and Si-Al_2O_3 contacts after cutting

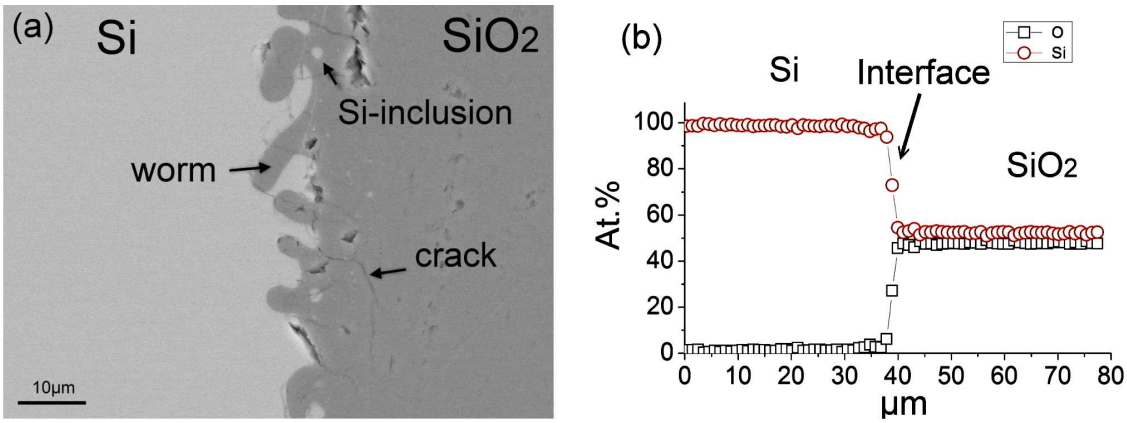

Figure 3. Backscattered SEM image (a) and EDS line scan (b) of the Si-SiO_2 contact

growth mechanism [8]. The original metastable SiO_2 dissolved in the Si melt to form a saturated reaction zone at the interface. After cooling, the Si inclusion and worm-like SiO_2 precipitated in the reaction zone. The EDS line scanning in Fig. 3b shows the Si- and O-concentration profiles for the Si-SiO_2 contact, indicating that elemental oxygen barely diffuses into the Si substrate. Figures 4a and 4b show the TEM bright-field (BFI) and dark-field images (DFIs) of the Si-SiO_2 contact after annealing at 1450 °C for 30 min. A large number of dislocations, a crack, and dislocation pile-ups appeared near the Si-SiO_2 interface. After contacting SiO_2 and Si, the oxygen diffused into the Si melt and an excess of oxygen atoms could be precipitated, causing stress that can easily induce dislocations and stacking faults [14]. Figure 4c shows the EDS line scan of the Si-SiO_2 contact. It was noted that the concentration of oxygen dissolved in the Si substrate is ≈3–20 at.% at a distance >1.25 μm from the interface. Figures 4d and 4e show the selected area diffraction patterns (SADPs) of the Si substrate (with a zone axis of [110]) and SiO_2, respectively. From the diffraction pattern of SiO_2 shown in Fig. 4e, a spot pattern is evident, and this supports the occurrence of cristobalite (SiO_2) crystallization at the interface.

Figure 5a presents the SEM BSI of the Si-Al_2O_3 contact, which shows no reactional phase or cracks at the interface contrasting that of the Si-SiO_2 contact in Fig. 3a. Figure 5b shows the EDS line scan of the Si-Al_2O_3 contact. It can be seen that Al and O barely diffuse into

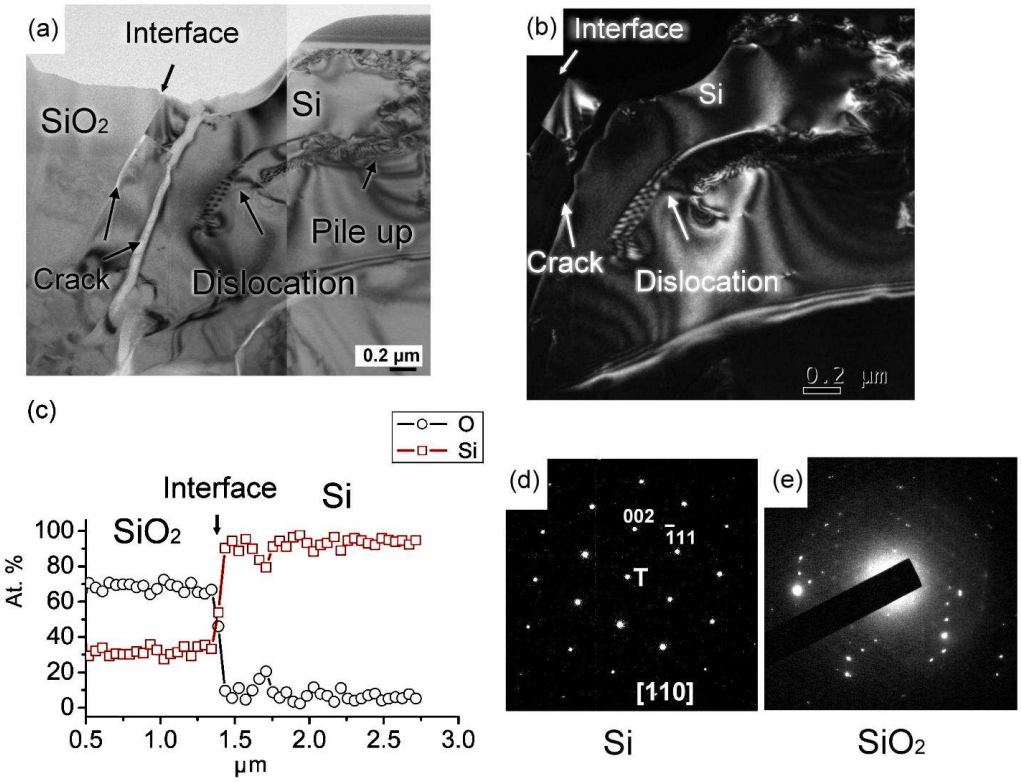

Figure 4. Bright-field TEM image (a), dark-field TEM image (b) and EDS line scan (c) of the Si-SiO_2 contact. Selected area diffraction patterns of Si with a zone axis of [110] (d) and SiO_2 (e)

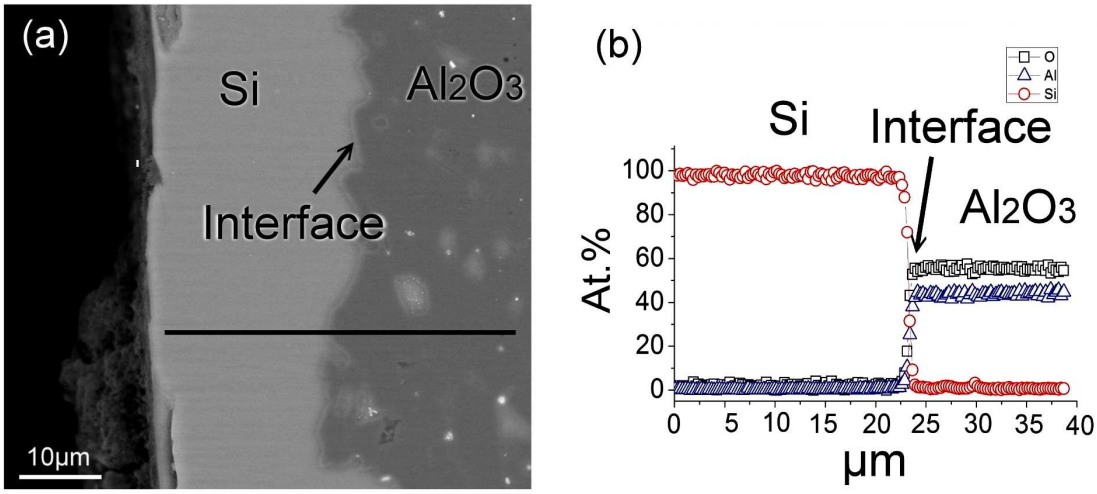

Figure 5. Backscattered SEM image (a) and EDS line scan (b) of the Si-Al_2O_3 contact

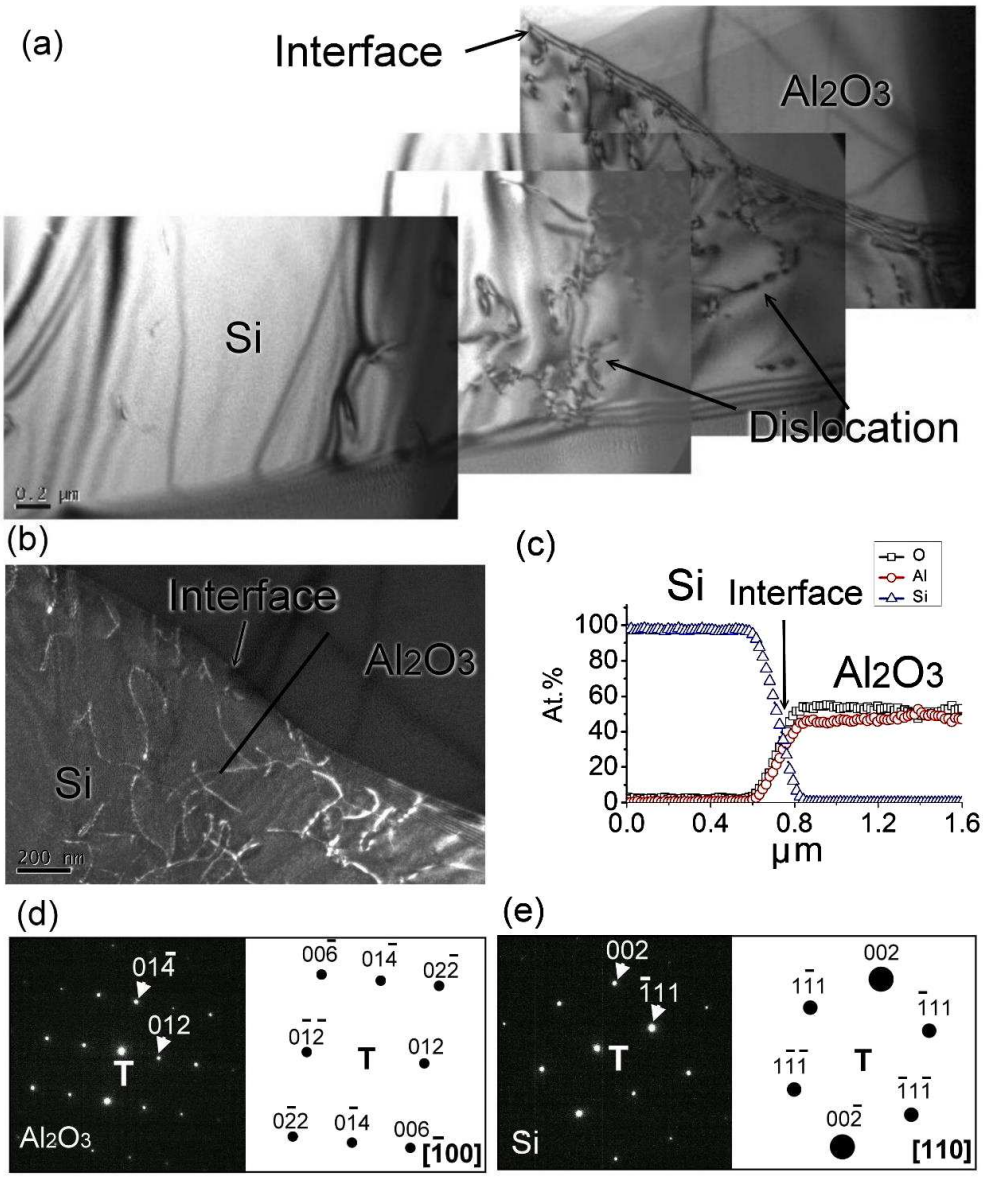

Figure 6. TEM BFI (a), DFI (b) and EDS line scanning (c) of the Si–Al2O3 contact. Experimental and simulated SADPs of Al2O3 with a zone axis of [100] (d) and Si with a zone axis of [110] (e)

the Si substrate. Figures 6a and 6b show the TEM BFI and DFI of the Si-Al_2O_3 contact, showing that dislocations gather at the interface and their number gradually decreases toward the Si side. It is believed that oxygen from the Al_2O_3 dissolved into the Si substrate, resulting in a stress increase, which induced the formation of dislocations near the Si-Al_2O_3 interface. Additionally, unlike the Si-SiO_2 contact shown in Fig. 4a, no cracks or dislocation pileups were found at the interface. Figure 6c shows the EDS line scan of the Si-Al_2O_3 contact. Obviously, elemental Al and O do not diffuse deeply into the substrate. The content of oxygen in the Si substrate in the region ≈1 μm from the interface is <2 at.% for the Si-Al_2O_3 contact in Fig. 6c, but it is >20 at.% for the Si-SiO_2 contact, as shown in Fig. 4c. Figures 6d and 6e depict the experimental and simulated SADPs of Al_2O_3 (with a zone axis of [$\bar{1}$00]) and Si (with a zone axis of [110]), respectively.

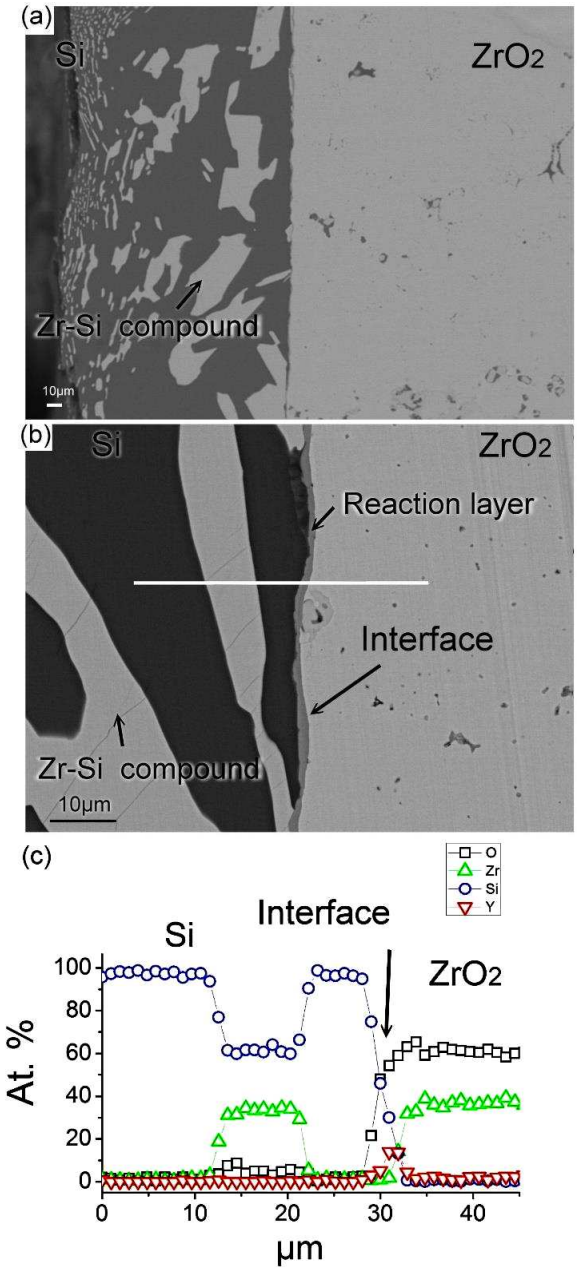

Figure 7. SEM BEI (a,b) and EDS line scan (c) of the Si-ZrO_2 contact from Fig. 7b

Figure 7a shows the SEM BEI of the Si-ZrO_2 contact, indicating a white reaction phase appearing in the Si substrate with a size gradually decreasing away from the interface toward the Si side. From the enlarged SEM BEI in Fig. 7b, a thin reaction layer can be clearly seen at the interface between Si and ZrO_2. From the EDS line scan of Fig. 7b, the white reaction phase comprises of ≈60 at.% Si and ≈40 at.% Zr, and a large amount of yttrium gathered in the thin reaction layer, as shown in Fig. 7c. When Si is in contact with ZrO_2, elemental Zr diffuses strongly into the Si substrate and reacts with Si to form a Zr-Si compound, the size of which decreases as Zr diffuses across the interface on the Si side. In addition, a large amount of elemental yttrium from the yttrium oxide (Y_2O_3) additive in ZrO_2 accumulated at the interface. Y_2O_3-stabilized ZrO_2 can exhibit increased mechanical strength and toughness. Obviously, elemental Y did not diffuse into the Si substrate but accumulated at the interface. The Zr-Si compound and yttrium-rich phase at the interface will be characterized and discussed in the following TEM analysis.

Figure 8a shows the TEM BFI of the Si-ZrO_2 contact, indicating a dislocation in the Si substrate and a reaction layer at the interface. From the EDS line scan of the Si-ZrO_2 interface (Fig. 8b), the composition of the reaction layer at the interface was corresponded to a $Y_2Si_2O_7$ phase (≈20 at.% Y, ≈20 at.% Si and ≈60 at.% O). The crystal structure of the $Y_2Si_2O_7$ phase was identified by the SADPs, shown in Fig. 8f. From the Y_2O_3-SiO_2 phase diagram [15], the YPS ($Y_2Si_2O_7$) and SiO_2 phases were found to coexist in the 0–30 at.% Y_2O_3 range. Thus, it is possible that $Y_2Si_2O_7$-formation mechanism can be expressed by Eqs. 1 and 2. The oxygen from ZrO_2 diffused into the Si substrate to form SiO_2 (Eq. 1) and then reacted with the Y_2O_3 in the ZrO_2 to produce $Y_2Si_2O_7$ (Eq. 2) at the Si-ZrO_2 interface. The evaluation of the Gibbs free energy (ΔG) for Eqs. 1 and 2 (calculated by HSC Chemistry version 6.0, Outotec Research Oy, Finland) is negative, proving that the formation mechanism is possible.

$$Si + O \rightarrow SiO_2,\ \Delta G_{1450\,^\circ C} = -885.8\,\text{kJ/mol} \quad (1)$$

$$SiO_2 + Y_2O_3 \rightarrow Y_2Si_2O_7,\ \Delta G_{1450\,^\circ C} = -50.6\,\text{kJ/mol} \quad (2)$$

In addition, it was noted that the Y concentration in ZrO_2 near the interface is ≈8–10 at.%, which was significantly higher than that away from the interface (≈1–3 at.%), as shown in Fig. 8b. From compositional analysis, the ZrO_2 with a high Y content (≈8–9 at.%) could be cubic ZrO_2 (c-ZrO_2) and that away from the interface could be tetragonal ZrO2 (t-ZrO_2). According to the ZrO_2-Y_2O_3 phase diagram [16], the additive of Y_2O_3, acting as stabilizer, in ZrO_2 will enhance the formation of the cubic ZrO_2. In addition, a strain field is

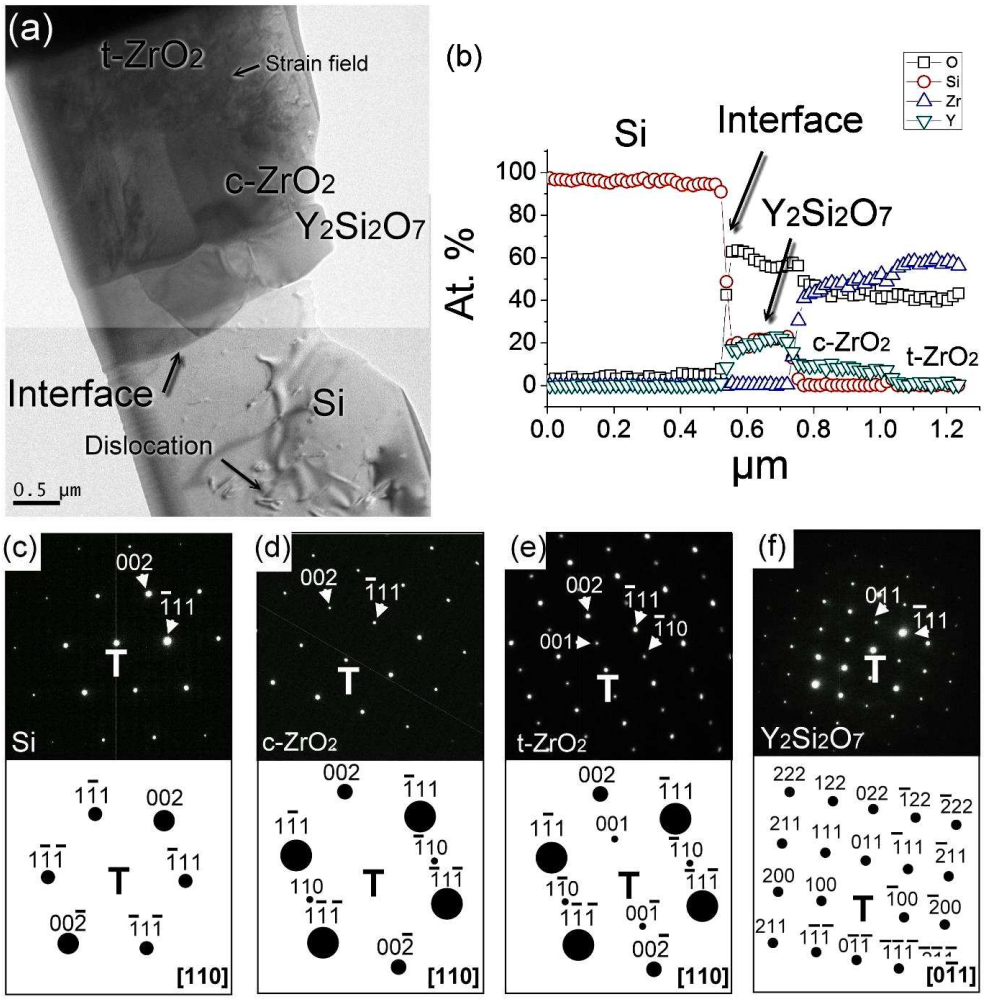

Figure 8. TEM BFI (a) and EDS line scan (b) of the Si-ZrO_2 contact. Experimental and simulated SADPs of: c) Si with a zone axis of [110], d) c-ZrO_2 with a zone axis of [110], e) t-ZrO_2 with a zone axis of [110], and f) $Y_2Si_2O_7$ with a zone axis of [0$\bar{1}$1]

found in the t-ZrO_2 phase, shown in Fig. 8a, because the tetragonal-to-monoclinic phase transformation is restrained [17]. Figures 8d and 8e show the experimental and simulated SADPs of c-ZrO_2 and t-ZrO_2 (both along the zone axes of [110]). Figure 8e indicates a 001 spot appearing in the SADP of t-ZrO_2. Reflections of the type odd, odd, even (which are not allowed for c-ZrO_2) were applied extensively to distinguish the c-ZrO_2 from the t-ZrO_2 phase [18,19].

Figure 9a shows the TEM BFI of $ZrSi_2$ within the Si substrate (corresponding to the Zr-Si compound in the SEM shown in Fig. 7b). As indicated by point 3 and 4 of the EDS point analysis of the data in Fig. 9a (shown in Fig. 9b), the composition of the Si-Zr compound corresponds to $ZrSi_2$. The structural identification of the $ZrSi_2$ crystal was supported by SADPs. Simulated patterns with zone axes of [201] and [101] are shown in Figs. 9c and 9d, respectively. The $ZrSi_2$ reaction mechanism can be described by Eq. 3 and the Gibbs free energy was negative (as calculated by HSC Chemistry version 6.0). When Si was put into contact with ZrO_2 at 1450 °C, the Zr from the ZrO_2 diffused and reacted with the Si substrate to form $ZrSi_2$ after cooling. In addition, the size of the $ZrSi_2$ gradually decreased away from the interface on the Si side due to the gradually decreasing concentration of Zr away from the interface on the Si side.

$$\mathrm{Zr} + 2\,\mathrm{Si} \rightarrow \mathrm{ZrSi_2},\ \Delta G_{1450\,^\circ\mathrm{C}} = -138.4\,\mathrm{kJ/mol} \quad (3)$$

For the oxygen content and resistivity measurements, after the contact between the Si and the ceramics several pieces (≈800 μm in thickness) of Si were cut along the direction longitudinal to the interface as shown in Fig. 1b. Figure 10a shows the distributions of the oxygen concentration in the Si pieces moving away from the interface of Si-SiO_2, Si-Al_2O_3 and Si-ZrO_2 dissolution couples, as measured via FTIR. The oxygen from the ceramics easily diffused into the Si substrate, supported by the evaluation of diffusivity for different elements in Si. The diffusivity of Al (5.198×10^{-1} cm^2/s [20]), Y (8.145×10^{-3} cm^2/s [21]), Si (4.199×10^{2} cm^2/s [22]) and O (8.567×10^{1} cm^2/s [23]) in Si substrate was evaluated at 1200 °C, respectively. The results indicated that Si and O easily diffused into Si substrate compared with Al and Y. Besides, the solubility of both Y and Zr

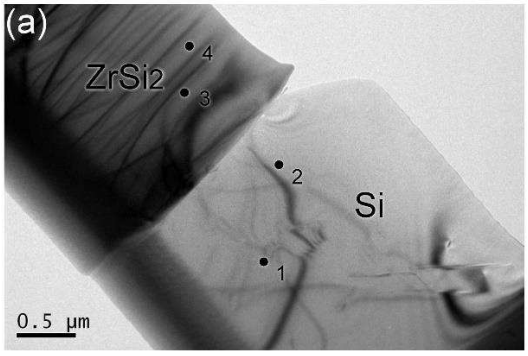

(b)

Point	Composition(at.%) 1	2	3	4
Si	96.13	95.77	64.25	65.26
Zr	---	---	35.75	34.74
O	3.87	4.23	---	---
Phase	Si	Si	$ZrSi_2$	$ZrSi_2$

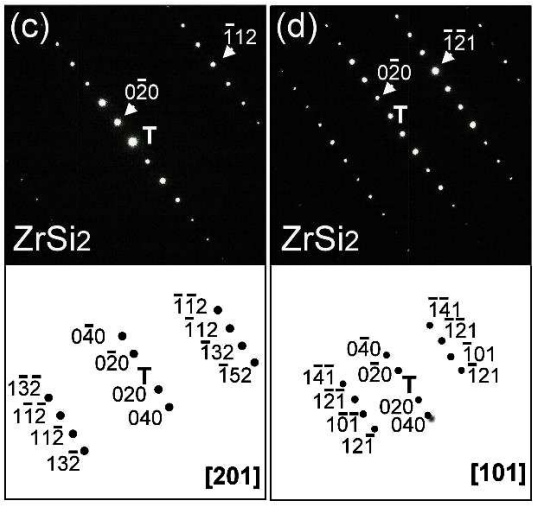

Figure 9. TEM BFI (a) and EDS point analysis (b) of $ZrSi_2$ within the Si substrate. Experimental and simulated SADPs with a zone axis of: c) [201] and d) [101]

in solid silicon is negligible comparing with that of O in Si. For all dissolution couples, the oxygen concentration near the interface was high and gradually decreased away from the interface in Fig. 10a. The highest oxygen concentration in Si was $\approx 5.68 \times 10^{17}$ atoms/cm^3 near the interface of the Si-Al_2O_3 dissolution couple. About 2.4 mm away from the interface (piece 3), the oxygen concentration was similar for all dissolution couples at around $\pm 1 \times 10^{17}$ atoms/cm^3. The oxygen concentration in the Si was 10.5–13.2 $\times 10^{17}$ atoms/cm^3 (12–15 ppm) before the contact with the ceramics. The oxygen concentration of Si decreased for all Si-ceramics dissolution couples, probably caused by the SiO gas evaporation during the heat treatment.

Figure 10b shows the electrical resistivity of the Si pieces moving away from the interface of Si-SiO_2, Si-Al_2O_3 and Si-ZrO_2 dissolution couples, as measured via four-point probe resistance meter. Similarly, for all dissolution couples the electrical resistivity near the interface was high and gradually decreased away from the interface. Taking the Si-SiO_2 dissolution couple as an example, the resistivity near the interface was about 0.55 Ω·cm and decreased to as low as 0.38 Ω·cm away from the interface. The resistivity of Si was measured as 21.85 Ω·cm before the contact with the ceramics. As anticipated, the resistivity of Si close to or away from the Si-ceramics interface decreased in comparison with that of pure Si. Hull indicated [24] that the unintentional oxygen diffusion in Si usually manifests itself as n-type doping (with SiO_4 as the donor) and easily results in a decrease in the resistivity of Si. When Si came into contact with ceramics, the oxygen from the ceramics could diffuse into the Si, causing a decrease in its resistivity. This was supported by the resistivity measurements shown in Fig. 10b. Furthermore, when the Al atom from Al_2O_3 replaces a Si atom in the silicon substrate, the remaining valence electrons are insufficient to satisfy the four covalent neighbouring bonds of Si resulting in the formation of the holes. Thus, the Al (IIIA) atom is acceptor. As for the Zr and Si originating from the ceramics into the Si substrate, the electrical property of the Si substrate could not be effectively changed due to the

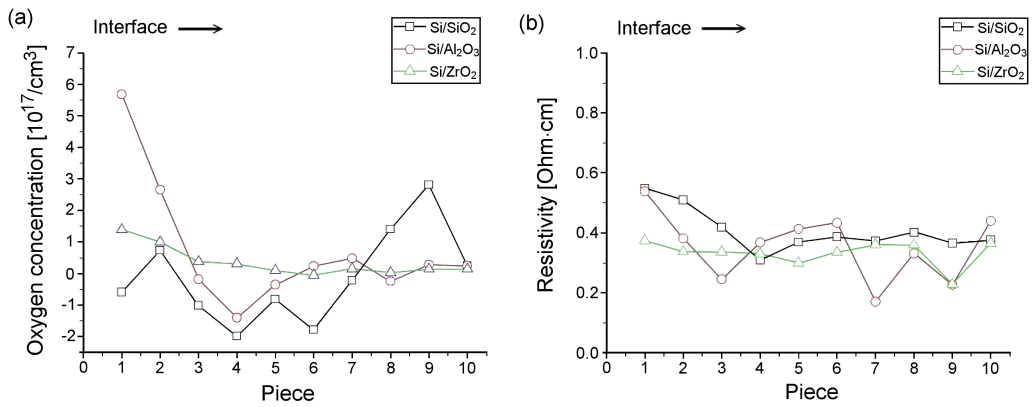

Figure 10. The vertical oxygen concentration (a) and electrical resistivity distribution (b) of Si pieces away from the interface of Si-SiO_2, Si-Al_2O_3 and Si-ZrO_2 dissolution couples

charge balance effect (Si^{4+} = Zr^{4+}). However, the dissolution of the impurities of Zr, Al, O and Y into the Si substrate could result in the interstitial or vacancies defects thus affecting the electrical resistivity.

IV. Conclusions

Reactions between different kinds of ceramics and silicon were studied to evaluate ceramics as candidates for their use in the process of silicon-crystal growth.

1. After bringing SiO_2 and Si into contact with one another, the original SiO_2 dissolved into the Si melt to form a saturated reaction zone at the interface. After cooling, Si inclusions and worm-like SiO_2 precipitated in the reaction zone near the interface. A large number of dislocations, a crack, and dislocation pile-ups appeared near the Si-SiO_2 interface. Oxygen diffused into the Si melt, and an excess of oxygen atoms could be precipitated, causing stress that can easily induce dislocations and stacking faults. In addition, the concentration of oxygen dissolved in the Si substrate was ~3–20 at.% by EDS of TEM near the interface.
2. In the Si-Al_2O_3 dissolution couple, the oxygen in Al_2O_3 diffused into the Si side, which resulted in a large number of dislocations in the Si. No obvious cracks or dislocation pile-ups were found at the interface in comparison to the Si-SiO_2 dissolution couple. Comparing the oxygen concentration in the Si substrate in the region around 1 μm from the interface with that at the interface, it was <2 at.%, determined by EDS of TEM in the Si-Al_2O_3 dissolution couple.
3. For the Si-ZrO_2 dissolution couple, elemental O and Y from the ZrO_2 diffused and reacted with Si to form a reaction layer, $Y_2Si_2O_7$. The ZrO_2 near the $Y_2Si_2O_7$ layer is cubic ZrO_2 because of the aggregation of ≈8–9 at.% yttrium. Away from the cubic ZrO_2, the ZrO_2 changed to tetragonal ZrO_2 because of low levels of yttrium ≈2–3 at.%. In addition, the Zr of the ZrO_2 diffused into the Si substrate, resulting in the formation of $ZrSi_2$. The size of $ZrSi_2$ gradually decreased away from the interface.
4. After contact between the Si and the ceramics, for all dissolution couples the oxygen concentration near the interface was high and gradually decreased away from the interface. The highest oxygen concentration in Si was $\approx 5.68 \times 10^{17}$ atoms/cm^3 for the Si-Al_2O_3 dissolution couple. Similarly, for all dissolution couples, the electrical resistivity near the interface was high and gradually decreased away from the interface. When Si came into the contact with ceramics, the oxygen from the ceramics could be easily diffused into the Si which resulted in a decrease in the resistivity of Si.

References

1. L. Válek J. Šik, "Defect engineering during Czochralski crystal growth and silicon wafer manufacturing", *Modern Aspects of Bulk Crystal and Thin Film Preparation*, Ed. N. Kolesnikov, InTech, 2012.
2. D.H. Hwang, B.Y. Lee, H.D. Yoo, O.J. Kwon, "Anomalous oxygen precipitation near the vacancy and interstitial boundary in CZ-Si wafers", *J. Cryst. Growth*, **213** (2000) 57–62.
3. M. Itsumi, "Octahedral void defects in Czochralski silicon", *J. Cryst. Growth*, **237** (2002) 1773–1778.
4. J. Furukawa, H. Tanaka, Y. Nakada, N. Ono, H. Shiraki, "Investigation on grown-in defects in CZ-Si crystal under slow pulling rate", *J. Cryst. Growth*, **210** (2000) 26–30.
5. T. Minami, S. Maeda, M. Higasa, K. Kashima, "In-situ observation of bubble formation at silicon melt-silica glass interface", *J. Cryst. Growth*, **318** (2011) 196–199.
6. J. Xu, W. Wang, D. Yang, H.J. Moeller, "Transmission electron microscopy investigation of the micro-defects in Czochralski silicon", *J. Alloy Compd.*, **478** (2009) 758–762.
7. A. Lanterne, G. Gaspar, Y. Hu, E. Øvrelid, M.D. Sabatino, "Characterization of the loss of the dislocation-free growth during Czochralski silicon pulling", *J. Cryst. Growth*, **458** (2017) 120–127.
8. S.M. Schnurre, R. Schmid-Fetzer, "Reactions at the liquid silicon/silica glass interface", *J. Cryst. Growth*, **250** (2013) 370–381.
9. X. Huang, S. Koh, K. Wu, M. Chen, T. Hoshikawa, K. Hoshikawa, S. Uda, "Reaction at the interface between Si melt and a Ba-doped silica crucible", *J. Cryst. Growth*, **277** (2003) 154–161.
10. X. Huang, T. Hoshikawa, S. Uda, "Analysis of the reaction at the interface between Si melt and Ba-doped silica glass", *J. Cryst. Growth*, **306** (2007) 422–427.
11. R. Kvande, L. Arnberg, C. Martin, "Influence of crucible and coating quality on the properties of multicrystalline silicon for solar cells", *J. Cryst. Growth*, **311** (2009) 765–768.
12. G. Cliff, G.W. Lorimer, "The quantitative analysis of thin specimens", *J. Microscopy*, **103** (1975) 203–207.
13. ASTM Standard F 1188. *Standard Test Method for Interstitial Atomic Oxygen Content of Silicon by Infrared Absorption*. ASTM International, West Conshohocken, PA, 2003.
14. M. Nikl, D. Nižanský, J. Ruzicka, C. Cannas, T. Yanagida, "Silicate glass-based nanocomposite scintillators", *Advances in Nanocomposite Technology*. Ed. A. Hashim, InTech, 2011.
15. E. Courcot, F. Rebillat, F. Teyssandier, C.L. Pouillerie, "Thermochemical stability of the Y_2O_3-SiO_2 system", *J. Eur. Ceram. Soc.*, **30** (2010) 905–910.
16. A. Dudek, "Microstructure and properties of the composites: Hydroxyapatite with addition of zirconia phase", *ASME. J. Eng. Mater. Technol.*, **133** [2] (2011) 021006.
17. K.L. Lin, C.C. Lin, "Reaction between titanium and zirconia powders during sintering at 1500 °C", *J. Am. Ceram. Soc.*, **90** (2007) 2220–2225.
18. K.L. Lin, C.C. Lin, "Zirconia-related phases in the zirconia/titanium diffusion couple after annealing at 1100–1550 °C", *J. Am. Ceram. Soc.*, **88** [10] (2005) 2928–2934.
19. M. Rühle, N. Claussen, A.H. Heuer, "Microstructural studies of Y_2O_3-containing tetragonal ZrO_2 polycrystals (Y-TZP)", pp. 352–370 in *Advances in Ceramics*, Vol. 12, *Science and Technology of Zirconia II*, Eds. N. Claussen, M. Rühle, A.H. Heuer. American Ceramic Society, Columbus, OH, 1984.

20. D. Navon, V. Chernyshov, "Retrograde solubility of aluminum in silicon", *J. Appl. Phys.*, **28** (1957) 823–824.
21. D.E. Nazyrov, M.I. Bazarbaev, A.A. Iminov, "Diffusion of yittrium in silicon", *Semiconductors*, **40** (2006) 768–769.
22. R.F. Peart, "Self diffusion in intrinsic silicon", *Phys. Stat. Solidi*, **15** (1966) K119–K122.
23. R.A. Logan, A.J. Peters, "Diffusion of oxygen in silicon", *J. Appl. Phys.*, **30** (1959) 1627–1630.
24. R. Hull, *Properties of Crystalline Silicon*, The Institution of Electrical Engineers, London, 1999.